J. metamorphic Geol., 2001, **19,** 217–231

Computer experiments to investigate complex fibre patterns in natural antitaxial strain fringes

D. KOEHN,[1] D. G. A. M. AERDEN,[2]* P. D. BONS[1] AND C. W. PASSCHIER[1]
[1]*Institut fuer Geowissenschaften, Johannes Gutenberg Universitaet, 55099 Mainz, Germany (koehn@mail.uni-mainz.de)*
[2]*Universidad de Salamanca Departamento de Geologia, Area de Geodinamica, Plaza de la Merced s/n, 37008 Salamanca, Spain*

ABSTRACT Antitaxial non-deforming strain fringes from Lourdes, France, show complex quartz, calcite and chlorite fibre patterns that grew around pyrite in a slate during non-coaxial progressive deformation. Development of these fringes was modelled using a computer program 'Fringe Growth 2.0' which can simulate incremental growth of crystal fibres around core-objects of variable shape. It uses object-centre paths as input, which are obtained from fibre patterns in thin section. The numerical experiments produced fibre patterns that show complex intergrowth of displacement-controlled, face-controlled and intermediate fibres similar to those in the natural examples. The direction of displacement-controlled growth is only dependent on the relative movement between core-object and fringe, so that core-object rotation with respect to the fringe influences the fibre patterns and produces characteristic asymmetric fibre curvature. Object-centre paths should be used for kinematic analysis of strain fringes instead of single fibres since these paths represent the fringe as a whole. The length along the path can be interpreted in terms of finite strain and path curvature in terms of rigid body rotation of fringes with respect to an external reference frame.

Key words: fibres; numerical experiments; strain analysis; strain fringe.

INTRODUCTION

Strain fringes are crystalline domains that occur alongside rigid objects such as porphyroblasts or clasts and which differ from the deformed rock matrix (Fig. 1). Fringes develop on the side of the extensional instantaneous stretching axes (ISA) of flow, and crystals that normally develop euhedral forms, such as quartz and calcite, tend to grow in a fibrous habit in these fringes (Muegge, 1928; Pabst, 1931). A core-object and its two strain fringes are termed a *fringe structure*. Fibrous crystals are of special interest to geologists since they can record not only finite strain but actual deformation paths; they grow progressively while the host rock is being deformed, so that they have been used to evaluate the deformation history of the host rock (e.g. Zwart & Oele, 1966; Elliot, 1972; Wickham, 1973; Wickham & Anthony, 1977; Cox & Etheridge, 1983; Sample & Fisher, 1986; Beutner *et al.*, 1988; Fisher, 1990; Spencer, 1991; Clark *et al.*, 1993; Fisher & Anastasio, 1994; Hedlund *et al.*, 1994).

Strain fringes have been classified into antitaxial, syntaxial, deforming or non-deforming fringes (reviews in Ramsay & Huber, 1983; Passchier & Trouw, 1996) depending on the direction of crystal growth and on their strength compared with the matrix. In this paper, we concentrate on the common antitaxial non-deforming type, where crystal growth takes place at the object–fringe interface and the fringes remain rigid and undeformed in the matrix. Antitaxial strain fringes are normally further divided into face-controlled or displacement-controlled fringes according to the geometry of fibre arrangement in the fringes (Ramsay & Huber, 1983; Passchier & Trouw, 1996). 'Face-controlled' means that fibres grow normal to the core-object face; 'displacement-controlled' means that they grow parallel to the relative displacement of fringes and core-object during progressive deformation. Koehn *et al.* (2000) suggested that these two groups are only end-member cases and that most fringes contain fibres of both groups (Fig. 1).

The main problems to be addressed in fibre analysis are: (1) why displacement-controlled fibres develop; (2) what they actually trace; and (3) how they can be used to determine the deformation history of the host rock. Present models suggest that: (a) fibres grow in the direction of the least principal stress (Durney & Ramsay, 1973); (b) they grow parallel to the incremental maximum extensional strain axis (Ellis, 1986; Kanagawa, 1996); (c) their growth is parallel to the orientation of the incremental maximum finite strain axis (Beutner & Diegel, 1985); or (d) that they follow points on the core-object and are not directly dependent on the orientation of either a strain or stress axis (Urai *et al.*, 1991; Aerden, 1996; Koehn *et al.*,

*Present address: Departmento de Geodinamica, Universidad de Granada, Campus de Fuentenueva s/n, 18071 Granada, Spain.

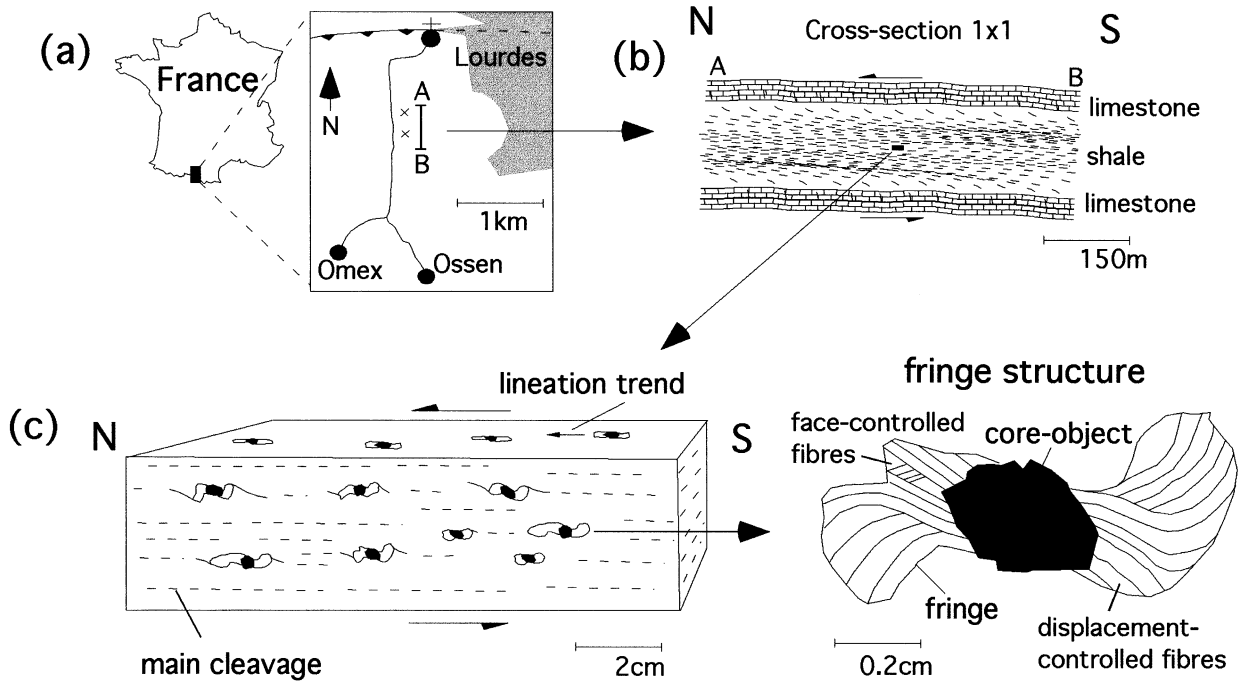

Fig. 1. (a) Map indicating the location of the studied samples. (b) The cross-section shows the slate unit containing the strain fringes between two massive limestone units. The cleavage is almost horizontal in the slate unit and is refracted by the limestone indicating strong deformation partitioning. (c) Line drawing of a hand specimen containing strain fringes from Lourdes, France, showing a consistent Z shape of the strain fringes that indicates top-to-the-north shear sense. Enlargement of one fringe structure shows curved displacement-controlled fibres and face-controlled fibres which grow perpendicular to the core-object surface.

2000). Koehn *et al.* (2000) suggested that the occurrence of juxtaposed displacement-controlled and face-controlled fibres means that the fibre growth direction is not directly dependent on either stress or strain, which supports the models of Urai *et al.* (1991) and Aerden (1996). Single displacement-controlled fibres can only be used for strain analysis in a few restricted cases where the core-object does not rotate with respect to the fringes, since core-object rotation influences the fibre patterns (Casey *et al.*, 1983; Aerden, 1996; Koehn *et al.*, 2000).

Aerden (1996) and Koehn *et al.* (2000) introduced 'object-centre paths' that can separate the opening paths of fringes from relative rotation of the core-object with respect to its fringes. The opening path of a fringe describes the movement of its oldest part away from the core-object during progressive deformation. Curved object-centre paths suggest a change in the opening direction of a fringe which might be due to rotation of the fringe structure with respect to ISA. An object-centre path can be determined from a scanned image of a thin section on which the core-object is superimposed using a graphics package. The superimposed core-object is then moved and rotated around its centre with respect to the fixed image in such a way that single points on the core-object follow displacement-controlled fibres in a fringe (Fig. 2). The line connecting the core-object centre positions during this procedure is termed the object-centre path. It is thought to represent the relative translation between the oldest fringe increment and the core-object. The relative rotation of a core-object with respect to its fringes can be indicated along the path as a variable angle of absolute rotation with respect to the initial orientation of the core-object (Fig. 2). If one fringe contains at least two displacement-controlled fibres, the object-centre path can be determined. The orientation of the opening vector of the fringe and the angle of the rotation of the core-object with respect to the fringe must have the same value for all displacement-controlled fibres in one fringe for one incremental opening step. The advantage of the object-centre path method is that the path represents one fringe as a whole and it distinguishes between the relative displacement of fringe and core-object, and their relative rotation (Koehn *et al.*, 2000).

Computer models of fibre growth in veins and strain fringes have been recently developed ('Vein Growth': Bons, in press; 'Fringe Growth': Koehn *et al.*, 2000). Using these models, Hilgers *et al.* (1997), Koehn *et al.* (2000) and Hilgers *et al.* (in press) demonstrated that the fibre growth theory of Urai *et al.* (1991) is able to explain simple fibre patterns in antitaxial strain fringes and veins. According to this growth theory, displacement-controlled or tracking fibres develop because they become locked to outward-pointing asperities on the core-object or on the vein wall-rock. The shape and roughness of the core-object surface or the vein wall-

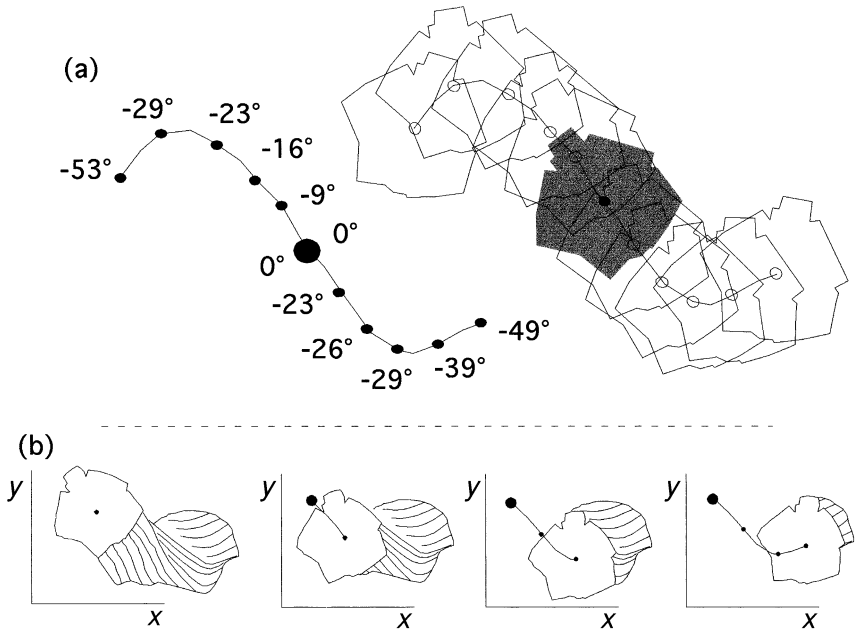

Fig. 2. (a) Interpretation of a fringe structure from Lourdes using the object-centre path method (Aerden, 1996; Koehn *et al.*, 2000). The core-object is progressively moved over a fringe and rotated around its centre so that displacement-controlled fibres follow points on the core-object surface. Relative finite rotation of the fringe and the core-object with respect to each other is indicated by the numbers next to the path. Anticlockwise rotation of the core-object around its centre with respect to a fixed fringe is positive. Different numbers on each side of the object-centre path represent different relative rotation of the two fringes. (b) Four-step evaluation of the object-centre path for the right-hand side fringe of (a).

rock therefore have a strong influence on the tracking ability of fibres. If this growth theory is valid for all veins and fringe structures, then strain analysis using single fibres should not be applied because it is prone to produce large errors since: (a) not all fibres in a fringe may track displacement; and (b) core-object rotation relative to its fringes results in complex fibre curvature (Koehn *et al.*, 2000). Instead, object-centre paths should be determined from natural strain fringes which can be used to investigate finite and incremental strain.

In this study, we used version 2.0 of the computer program 'Fringe Growth' (Koehn *et al.*, 2000) to simulate fibre growth in strain fringes from a locality in the northern Pyrenees near Lourdes, France. 'Fringe Growth' models fibre growth on a rigid core-object of any shape by varying the fringe displacement rate, rotation and several other parameters. The strain fringes from Lourdes show very complex fibre patterns formed during non-coaxial progressive deformation around pyrite grains of variable shape (Fig. 1). They are ideal to test whether 'Fringe Growth' can reproduce these patterns and whether the fibre growth theory of Urai *et al.* (1991) is a realistic model for the development of fringe structures. To do this, object-centre paths were determined from four differently shaped fringe structures and were used in 'Fringe Growth 2.0' to simulate the fibre patterns. The simulated strain fringes were then compared with the natural examples. In order to improve the understanding of the development of displacement-controlled, face-controlled and other fibre types, incremental fibre growth was examined in detail. This made it possible to establish an enhanced classification for different fibre types. Finally, a method was developed to interpret object-centre paths in terms of finite and incremental strain and in terms of fringe rotation with respect to ISA, and this method is applied to the fringe structures from Lourdes.

GEOLOGICAL SETTING

The study area lies in the Pyrenees, north of the North Pyrenean fault (for details, see Aerden, 1996, and references therein) in the south of France (Fig. 1a). The strain fringes occur in a 150 m thick layer of Cretaceous slate between two 50–100 m thick Cretaceous limestone beds (Fig. 1b). The whole sequence is folded into kilometre-scale north-verging folds and is cut by north-directed thrusts (Aerden, 1996). The main sample location for the strain fringes used in this study lies about 1 km south of a major thrust at Lourdes where the sequence dips gently to the south (Fig. 1b). In this area, the slate unit experienced strong internal deformation between the limestone units with a strong flat-lying cleavage and isoclinal folds. The two limestone units above and below the slate are little deformed. The cleavage shows a strong refraction towards the limestone units: it dips about 0° to 20°

towards the south in the slate and about 50° to 75° towards the south in the limestone (Fig. 1b).

The strain fringes show a strong linear elongation trending north–south on cleavage planes without any evidence for extension perpendicular to the lineation during fringe growth (Fig. 1c). On west-facing outcrop surfaces oriented perpendicular to the cleavage, the strain fringes show a consistent Z shape indicating a top-to-the-north sense of shear (Fig. 1c). This geometry infers that the strain fringes and the core-objects have all rotated sinistrally in this outcrop with respect to the limestone layers. Because of this rotation, the strong deformation partitioning in the slate and weak deformation of the limestone layers, we concluded that flow in the shear zone (slate unit) must have been close to simple shear.

In thin section, strain fringes with a length of 0.5–2.0 cm show antitaxial growth of quartz, calcite and chlorite fibres around pyrite of variable shapes (Fig. 1c). The mineralogy of the fibres seems to have no significant influence on the fibre shape. Fibres in the fringes show no sign of deformation or recrystallization, which suggests that their present geometry developed solely during growth. Single fibres can be curved up to 100° and are often truncated by suture lines. The fringes show complex intergrowth of displacement-controlled, face-controlled and other fibre types (Fig. 1c). Recent Rb–Sr dating of strain fringes from the same outcrop has established a long growth history from 85 to 55 Ma (Mueller *et al.*, 2000), which demonstrates the long-lived nature of the shear zone that hosts the fringes.

THE PROGRAM 'FRINGE GROWTH'

General description

Numerical experiments presented in this study were carried out with the computer model 'Fringe Growth 2.0'. The algorithm of this computer program is based on the program 'Vein Growth' by Bons (in press). 'Fringe Growth' is described in detail in Koehn *et al.* (2000) and is written in 'C' for the Macintosh computer. 'Fringe Growth 2.0' models the growth of fibres in antitaxial non-deforming strain fringes. The user can define the growth velocity of the fibres, the anisotropy of the crystal lattice in the fibres, the opening direction and opening velocity of the fringe and the relative rotation of the core-object with respect to the fringe. Only one fringe is simulated during each program run with the fringe fixed in the xy frame of the computer screen, while the core-object can move in x–y space on the computer screen and can rotate with respect to the fringe. The boundary of the model lies between the matrix and the strain fringe, so that matrix deformation is not included in the simulation (Fig. 3a). 'Fringe Growth 2.0' is a front-tracking model: the grains in the fringe and the core-object are defined by a number of nodes that connect straight segments defining the grain boundaries (details described in Koehn *et al.*, 2000). Triple nodes lie on the vertices between three neighbouring grains and double nodes between two neighbouring grains. Growth takes place by incremental movement of the nodes. A detailed description of the growth routine is given in Bons (in press). Two new features have been added to the version of 'Fringe Growth' presented in Koehn *et al.* (2000): the nucleation of new crystals inside the fringe (Fig. 3b) and the dissolution of crystals (Fig. 3c).

Nucleation inside the fringe

Observations in thin sections of strain fringes from Lourdes have shown that displacement-controlled fibres can contain face-controlled fibres on the fringe rims (Koehn *et al.*, 1999) as well as inside the fringes. These displacement-controlled fibres are termed *fibre bands* and can only develop if new grains nucleate on the fringe rims and inside the fringe between the core-object and the growing fibres. The program mimics this by randomly nucleating new grains at triple points on the growth interface of the fringe between two fibres that have a minimum width (Fig. 3b). The minimum width is defined as a grain that has at least two double nodes on its growing surface.

Dissolution of crystals

Because of the rotation and curved movement path of the core-object with respect to its fringes, parts of the core-object tend to overlap with parts of the fringe (Koehn *et al.*, 2000). In nature, this must either influence the path and rotation of the core-object, or parts of the fringe will be dissolved, bent or fractured. Since no fracturing or bending of fibres is observed in the fringe structures from Lourdes, dissolution of small parts of the fringes seems to be the dominant mechanism to overcome space problems. The crystals in 'Fringe Growth 2.0' are 'dissolved' by 'growing backwards' into themselves once parts of the core-object move over them (Fig. 3c). Single grains are removed from the fringes once they reach a critical minimum size as a result of the dissolution process. The critical minimum size of a grain that is removed from the fringe is defined as a grain that consists only of triple nodes without any double nodes.

EXPERIMENTS

Reproduction of fibre patterns in four samples (samples I–IV) from Lourdes (shown in Fig. 4a) was attempted using core-objects with axial ratios that range from 1.0 (sample I and sample II) to 1.4 (sample III) and 2.0 (sample IV). We determined the object-centre paths of the four samples (Fig. 4b) and used these and the core-object shape as an input for the simulations.

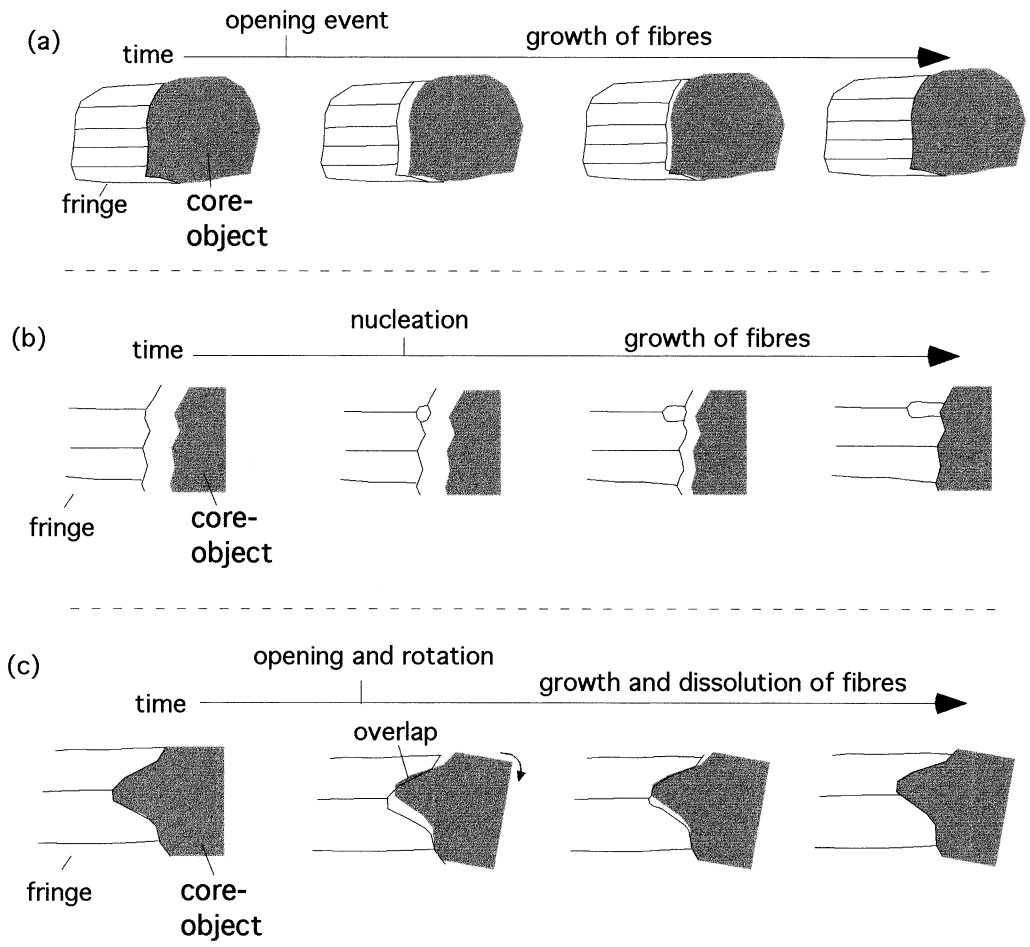

Fig. 3. Three versions of a single growth cycle in the program 'Fringe Growth'. (a) Opening of the fringe is followed by progressive growth of fibres in the open fringe towards the core-object. (b) A new nucleus is inserted at the growth interface of the fringe between two fibres. (c) Rotation of a core-object with pronounced corners leads to an overlap of core-object and fringe. Fibres that are overlapped by the core-object dissolve.

General results of the experiments

The fibre patterns in the simulated strain fringes (Fig. 4c) show the following similarities to the natural examples: (1) single fibres curve up to 100°; (2) fringes show complex intergrowth of different fibre types; (3) curvature of fibres changes along individual fibres; (4) fibres growing next to each other do not necessarily have the same curvature; (5) none of the fibres is parallel to an object-centre path along its whole length; and (6) fringes develop multiple suture lines (Ramsay & Huber, 1983) that separate sets of differently oriented fibres.

The four sets of natural fringes (and the simulated ones) each have a slightly different geometry (Fig. 4). The reason for this can be observed by comparing the fringe structures: (1) the number of suture lines per fringe varies depending on how many pronounced corners the core-objects have; (2) the width of fibres differs depending on the roughness of the core-object surface; (3) sites of dominantly face-controlled or displacement-controlled fibre growth vary depending on the orientation of the core-object and on the roughness of its surface; and (4) the outline of the fringes differs depending on the geometry of the object-centre path and on the axial ratio, shape, orientation and size of the core-object.

The main differences between the simulated and natural strain fringes are (Fig. 4): (1) simulated fibres are not as thin as fibres in the natural examples; and (2) the outline of the fringes is not always the same. Thick fibres form since the roughness of the core-object surface used for the simulations is not as fine as that of the natural examples; the computer program is restricted to a maximum number of nodes (20 000–40 000) due to memory and time constraints. This results in a lower resolution of the simulated fringes (wider fibres) compared to the natural examples. The roughness of the core-object of sample IV is different from samples I–III because the natural examples also have different roughnesses (Fig. 4). The outline of the fringes cannot be modelled as the

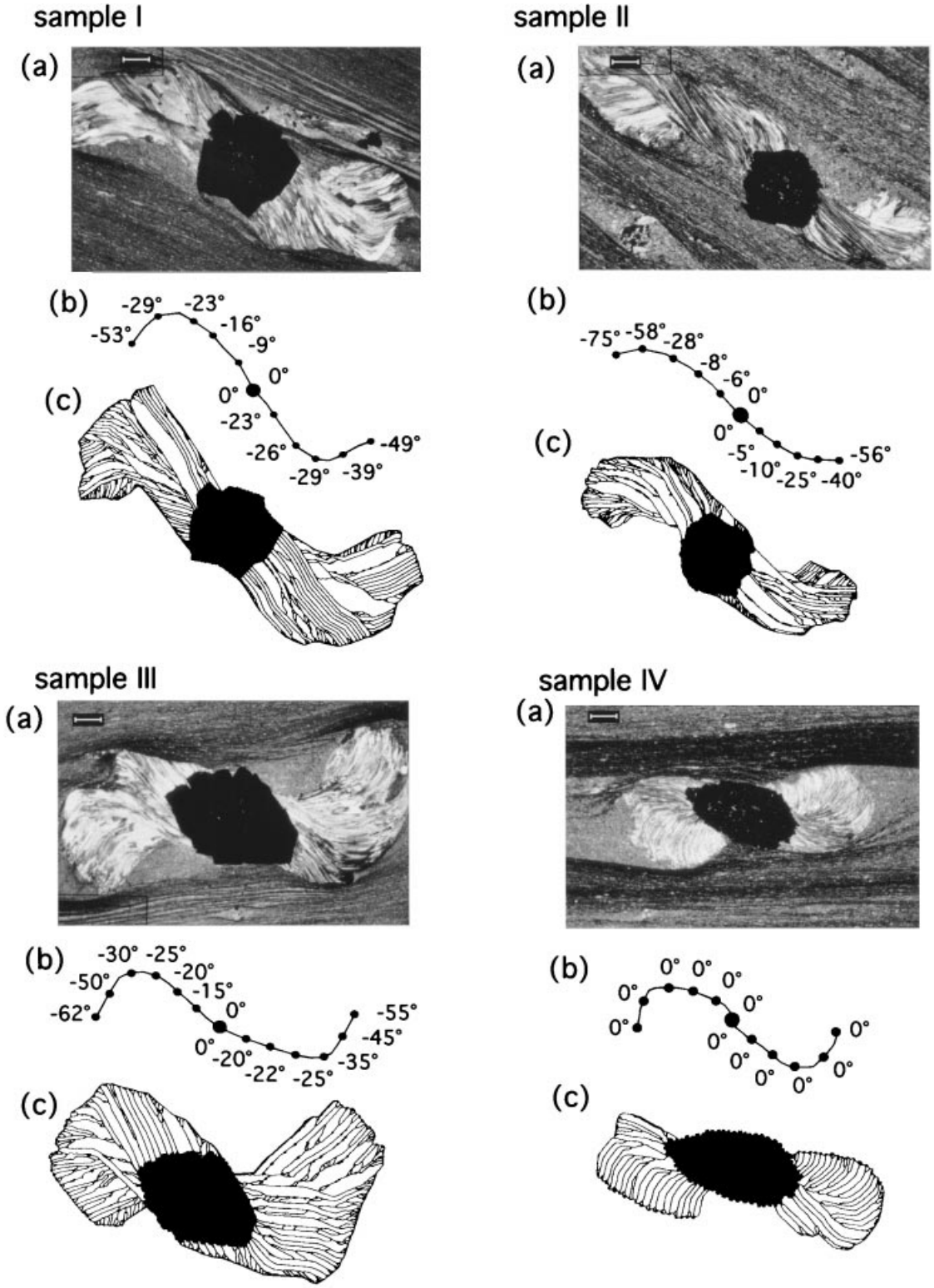

Fig. 4. (a) Thin section micrographs of the studied strain fringes. Scale bar is 0.8 mm. (b) Object-centre paths for the four strain fringes. (c) Simulated fringes around core-objects shown in (a). None of the fibres in the fringes is parallel to the object-centre path along its whole length. For a detailed discussion of the fibre patterns, see the main text.

outline is the boundary of the computer model. To model the outline of the fringes, deformation of the matrix would have to be included in the simulations, since we do not know how wide a fringe will be with respect to its core-object. Fringes next to a core-object will not open along the core-object's whole width (Fig. 4a) (Selkman, 1983).

As a general conclusion, the fibre patterns produced by the numerical experiments are very similar to the patterns observed in the natural examples (Fig. 4) which indicates that the fibre growth model of Urai *et al.* (1991) is realistic.

Because the experiments were able to mimic the internal geometry of the fringes quite well (Fig. 4), a detailed analysis of the evolution of specific fibre types can be undertaken. In the following paragraphs, fibre types are defined and treated separately to show which factors lead to the development of individual types and shapes.

Classification of fibre patterns

The numerical experiments show that fibre patterns in the fringes develop by complex intergrowth of face-controlled, displacement-controlled and intermediate fibre segments (Fig. 5). The shape of the fibre growth front determines which fibre type develops because fibre boundaries either get 'locked' to outward-pointing asperities on the core-object surface or grow perpendicular to this surface if it is flat (Urai *et al.*, 1991; Koehn *et al.*, 2000). An enhanced classification for fibres and fibre boundaries is suggested based on our numerical experiments (Fig. 5). Fibre *boundaries* can be either *displacement-controlled* (tracking), *face-controlled* (non-tracking) or *intermediate* (partial tracking). *Intermediate fibre boundaries* contain face-controlled and displacement-controlled segments along their length. *Displacement-controlled fibres* have two displacement-controlled fibre boundaries. *Suture lines* (Ramsay & Huber, 1983) represent a special kind of fibre boundary. They separate sets of differently oriented fibres in a fringe. *Face-controlled fibres* have two face-controlled fibre boundaries. *Fibre bands* are sets of face-controlled fibres within a displacement-controlled fibre (Fig. 5). *Intermediate fibres* are either made up of one displacement-controlled fibre boundary and one face-controlled fibre boundary or they are made up of intermediate fibre boundaries (Fig. 5). It is difficult to detect intermediate fibre boundaries in natural strain fringes and to identify their displacement-controlled and face-controlled parts.

Displacement-controlled (tracking) fibre boundaries

Displacement-controlled fibre boundaries in the fringes track asperities on the surface of the core-object. The width of displacement-controlled fibres depends mainly on the minimum distance between asperities of sufficient pointedness to capture fibre boundaries

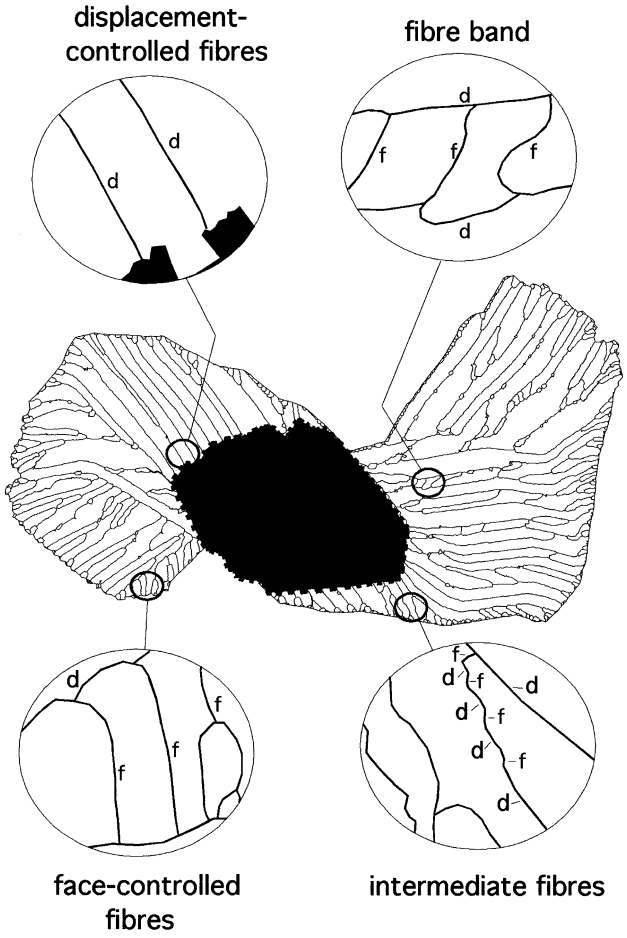

Fig. 5. Classification suggested for fibres and fibre boundaries illustrated by the simulated fibre patterns of sample III. f = face-controlled fibre boundary; d = displacement-controlled fibre boundary.

(Hilgers *et al.*, in press). The growth direction of displacement-controlled fibres is a function of: (1) the instantaneous opening direction between fringe and core-object (recorded by the object-centre path); and (2) the rotation of the core-object with respect to the fringe (indicated in numbers along the object-centre path). Displacement-controlled fibres in a fringe will all grow parallel to each other and parallel to the object-centre path only if the core-object is *not* rotating with respect to the fringe. Rotation of the core-object with respect to its fringe produces complex fibre patterns where single fibres change their curvature along the fibre's length even if the core-object rotation with respect to the fringe is constant (Fig. 6). In this case, fibre segments of the same age grow in different directions depending on the growth site of the fibre with respect to the centre of rotation (centre of the core-object) (Fig. 6). The more elongate the core-object is and the more it rotates with respect to the fringes, the more complex the fibre patterns will be. Our results show that such rotation of the core-object tends to

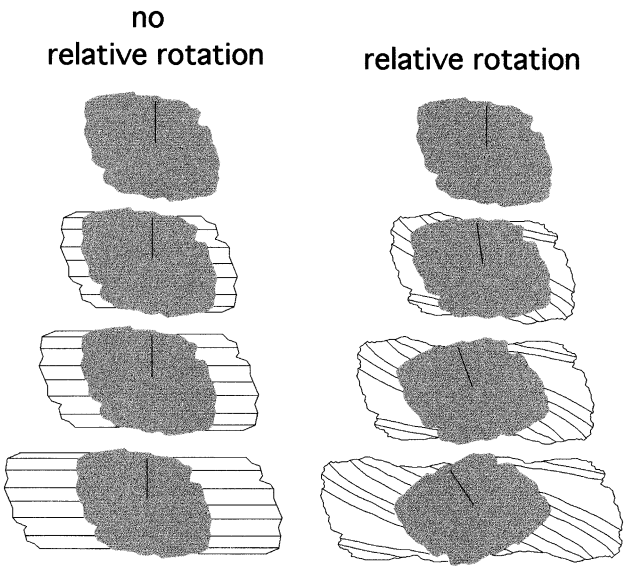

Fig. 6. Schematic drawing of displacement-controlled fibres after two simulations with the program 'Fringe Growth 2.0' with a constant opening vector parallel to the horizontal. Left-hand simulation shows growth of all displacement-controlled fibres parallel to each other, the core-object has not rotated relative to its fringes. Right-hand simulation shows different growth direction of fibres due to an anticlockwise rotation of the core-object relative to its fringes.

produce an asymmetric fibre curvature which results in fibre patterns that have an S or Z shape depending on the shear sense.

Figure 6 shows two series of line drawings of displacement-controlled fibres in a fringe simulated with 'Fringe Growth 2.0'. The object-centre path is straight and parallel to the horizontal during the simulations. At the left, the core-object does not rotate with respect to its fringes so that all fibres grow parallel to each other and parallel to the object-centre path (Fig. 6). At the right, an anticlockwise rotation of the core-object with respect to the fringe is induced and fibres of the same age have different growth directions depending on their position with respect to the core-object. Figure 7 illustrates a natural example of a strain fringe from Lourdes that shows single fibres that change their curvature from the upper right to the lower left rim of the fringe resulting in a Z shape. This Z shape indicates that the core-object rotated anti-clockwise with respect to its fringes.

For an infinitesimally small growth step of displacement-controlled fibres in one fringe, there is only *one* combination of opening and core-object rotation with respect to the fringe. Thus object-centre paths are unique for each fringe.

Suture lines

Suture lines in strain fringes (Ramsay & Huber, 1983) separate sets of differently oriented fibres. Suture lines are similar to displacement-controlled fibre boundaries

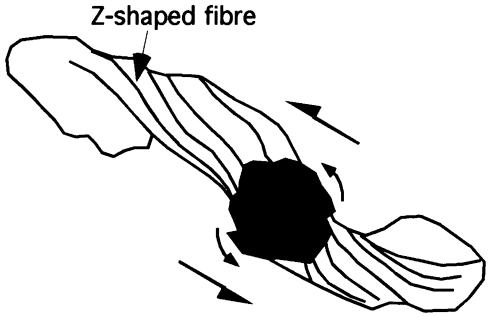

Fig. 7. Line drawing of some displacement-controlled fibres of sample II (Fig. 4) that have a typical asymmetric fibre curvature due to relative core-object fringe rotation. The Z-shaped fibres indicate that the core-object rotated anticlockwise relative to its fringes.

since they are also locked to asperities on the core-object surface but to first-order asperities (corners) rather than small, second-order ones described above. They can form because: (1) the core-object has pronounced corners; (2) the opening direction of the fringe changes suddenly; or (3) parts of the fringe are dissolved. Four common types of suture line can be distinguished (Fig. 8): (1) suture lines between sets of differently oriented face-controlled fibres; (2) suture lines between face-controlled and displacement-controlled fibres; (3) suture lines between displacement-controlled and intermediate fibres; and (4) suture lines between displacement-controlled fibres of different age.

Face-controlled (non-tracking) fibre boundaries and fibre bands

Face-controlled fibre boundaries grow on smooth core-object surfaces (Ramsay & Huber, 1983) where there are no asperities or only low-amplitude asperities that are unable to lock and thus unable to create displacement-controlled fibres (Koehn *et al*., 2000). These fibre boundaries can also occur inside fringes around rough core-objects (Koehn *et al*., 2000), where they are often found on the rims of fringes (Fig. 9a). In some cases, only one displacement-controlled fibre band contains face-controlled fibres in contrast to the neighbouring fibres (Fig. 9b). Displacement-controlled fibre bands can develop when a core-object has two distinct asperities that are separated by a smooth surface. The two asperities lock the outside boundaries of the fibre band which are therefore displacement-controlled. Nuclei inside the fibre band can grow face-controlled against the smooth surface and therefore grow oblique to the fibre band boundaries (Fig. 9c).

Intermediate (partially tracking) fibres

Purely face-controlled and purely displacement-controlled fibres are end-members because some single fibres, termed intermediate fibres, can have segments where one grain boundary is displacement-controlled

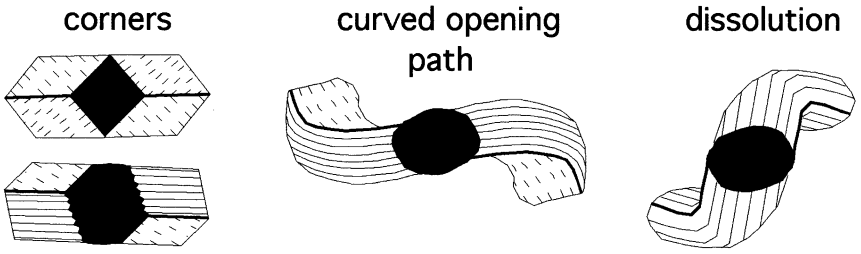

Fig. 8. Sketch of the different suture lines that are common in strain fringes. Face-controlled and intermediate fibre boundaries are indicated by broken lines.

and the other face-controlled, or where single grain boundaries switch between face- and displacement-controlled growth (intermediate fibre boundaries) (Fig. 10). This is commonly observed next to suture lines. Fibres that end on suture lines have to be treated with care, as they may be intermediate and rarely contain information on the opening path of the fringes. Figure 10(a, b) shows a two-step computer simulation of a Lourdes fringe. Figure 10(c) shows an enlarged area of Fig. 10(b) with intermediate fibres next to a suture line. The intermediate fibre boundaries switch progressively from face-controlled (labelled f in Fig. 10c) to displacement-controlled (labelled d in Fig. 10c) growth, so that the long axis of the intermediate fibre indicates neither a displacement- nor face-controlled growth direction (Fig. 10c). In addition, it is difficult to determine the exact age relationship of intermediate fibres next to a suture line if the orientation of the growth surface is not known and parts of the fringe have been dissolved.

INTERPRETATION OF OBJECT-CENTRE PATHS

Three parameters can be recognized in object-centre paths: (1) length along the path; (2) curvature of the path; and (3) core-object rotation relative to the fringes. The length along the path can be interpreted in terms of incremental and finite strain and the curvature gives an estimate of the absolute rotation of fringes with respect to an external reference frame if ISA orientation is constant during progressive deformation. Assuming that ISA orientation is constant, the curvature of object-centre paths results from: (a) rigid body rotation of fringes with respect to ISA; and (b) variations in fringe opening direction with respect to ISA.

The following sections contain an interpretation of the object-centre paths of samples I–IV (Fig. 4). In order to interpret the object-centre paths, three assumptions had to be made: (1) deformation in the studied shear zone was close to simple shear; (2) deformation was plane strain; and (3) fringes opened parallel to the extensional ISA. Assumptions (1) and (2) have been justified earlier in this paper. Assumption (3) seems justified since small fringes are pulled away from the core-object in the extensional ISA direction during early stages of fringe growth. However, assumption (3)

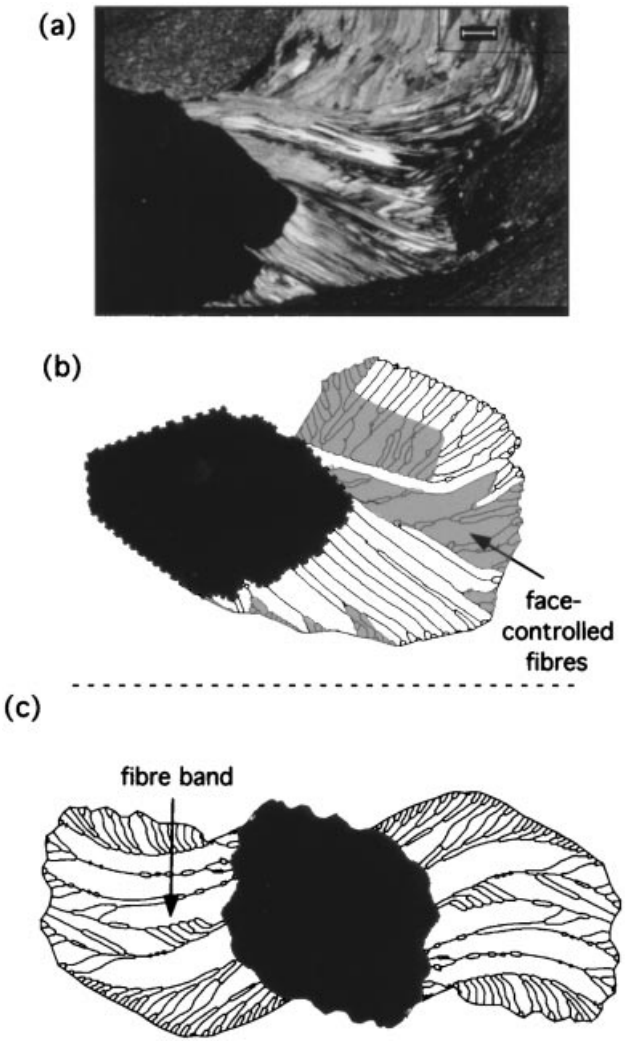

Fig. 9. (a) Natural strain fringe that shows face-controlled fibres next to a pronounced suture line and in displacement-controlled fibre bands. Scale bar is 0.8 mm. (b) Simulation of the natural example with 'Fringe Growth 2.0'. The fibre patterns of the natural and the simulated fringe are similar. Face-controlled and intermediate growing fibres are ornamented. A pronounced suture line separates displacement-controlled fibres from intermediate fibres. Fibre curvatures of neighbouring displacement-controlled fibres are not equal. (c) Simulation with 'Fringe Growth 2.0' that produced a displacement-controlled fibre band containing smaller face-controlled fibres next to large displacement-controlled fibres without internal fibres.

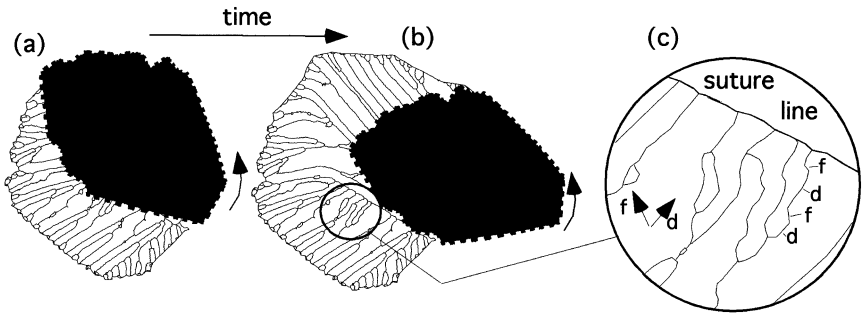

Fig. 10. Simulation with 'Fringe Growth 2.0' that produced intermediate fibres next to a suture line: (a) shows the position of the core-object during the growth of the intermediate fibres and (b) shows the development of the suture line. (c) Intermediate fibres with their typical patterns of f = face-controlled (non-tracking) parts and d = displacement-controlled (tracking) parts.

may be invalid for large fringe structures during late stages of fringe growth as examined in the Discussion section. On the basis that all assumptions are valid, the absolute rotation of fringes is plotted against shear strain in Fig. 11.

Incremental and finite strain

If the fringes open parallel to the extensional ISA, infinitesimally small object-centre path segments represent segments of infinitesimally small strain. To determine finite strain, integration is made along the object-centre path, since the finite length along the path does not represent finite strain but an accumulation of segments of 'incremental strain'. These segments of 'incremental strain' are only equal to the finite strain for the very first infinitesimally small fringe-opening step. Finite strain can be calculated from object-centre paths as follows. The Mohr circle for infinitesimal strain in the plane perpendicular to the cleavage and

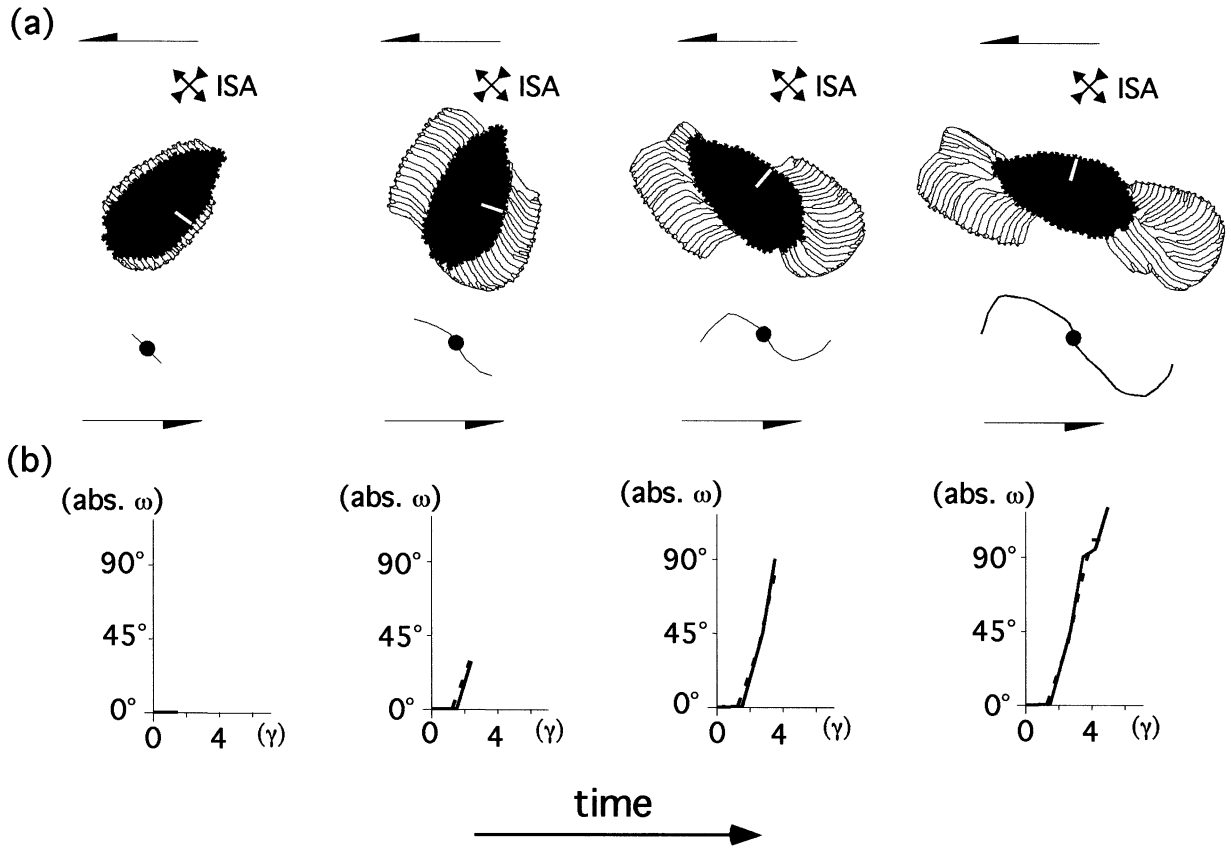

Fig. 11. (a) Progressive rotation of fringes, core-object and object-centre path with respect to ISA. The curvature of the object-centre path results from progressive rotation of older segments of the fringe. The outer segments of the object-centre path always contain the oldest growth increments, since object-centre paths grow from the centre (antitaxial growth in strain fringes). (b) The absolute rotation of fringes with respect to ISA can also be visualized in plots of absolute rotation versus shear strain where zero rotation is the orientation of the oldest segment of the object-centre path. The orientation of younger segments of the path is plotted with respect to the oldest segment. Broken line represents right fringe and solid line left fringe.

parallel to the lineation, assuming that the normal strain e_2 remains at zero (plane strain) (Means, 1976), shows that

$$\gamma_{max} = e_1 - e_3 \quad (1)$$

where γ is the shear strain and e_1 and e_3 are the normal strains with

$$e = \Delta l / l_0 \quad (2)$$

If the shear strain is infinitesimally small and the area remains constant, then

$$de_3 = -de_1 \text{ for } d\gamma \rightarrow 0 \quad (3)$$

so that

$$d\gamma_{max} = 2de_1 \text{ (for infinitesimally small strain)} \quad (4)$$

To calculate the finite shear strain, integration along the length of the object-centre path is undertaken:

$$d\gamma = 2de_1 = (2dl)/l_0 \quad (5)$$

where l is the incremental length of the object-centre path and l_0 is the diameter of the core-object. Integration gives:

$$\gamma_{finite} = \frac{2}{l_0} \int_0^L dl \Leftrightarrow \gamma_{finite} = \frac{2}{l_0} L \quad (6)$$

where L is the finite length measured along the object-centre path. Thus the shear strain along the shear zone can be determined from the object-centre path and indirectly from the displacement using the shear zone width. Note that l_0 varies if the core-object is elongate.

Results for the four strain fringes studied are shown in Fig. 12. The calculated shear strains have finite values of 5.0, 6.3, 7.6 and 9.8, so that the finite displacement along the 150 m thick shear zone studied would be between 750 m and 1420 m for the period during which the fringes grew. The shear strain values coincide with a small angle between the cleavage in the slate and the shear zone boundary of 5° to 10°. Etchecopar & Malavielle (1987) determined a shear strain of 6.0 for a fringe structure from the same shear zone using a computer program which includes matrix deformation.

Finite rotation of fringes with respect to an external reference frame

The curvature of the object-centre path can be used to estimate the progressive rotation of fringes with respect to the shear zone boundary or ISA if fringes open parallel to ISA. This applies in many cases but not always, as discussed below. The method is illustrated in Fig. 11 in four time steps, where Fig. 11(a) demonstrates the progressive rotation and growth of a fringe structure and the associated object-centre path with respect to ISA and Fig. 11(b) shows the corresponding plots of absolute rotation versus finite shear strain. The absolute rotation of the fringes is determined from the curvature of the object-centre path. Therefore, the absolute rotation of each incremental segment of the object-centre path is defined as the angle between this segment and the most distal and thus oldest part of the object-centre path. The finite rotation of fringes is represented by the curvature of the corresponding object-centre path.

Figure 12(b) shows plots of absolute rotation versus shear strain for samples I–IV. The gentle slopes of the curves in the plots during a shear strain of 0.0–2.0 indicate that all four strain fringes examined have a slow rotation rate during the first stages of their development. Steeper slopes of the curves during shear strains of 1.5 to about 4.0 indicate that the rotation rate increases. The rotation rates of fringes of samples I to III decrease during the late stages of fringe growth, illustrated by decreasing slopes of the curves. This could be due to the fact that the fringe structures treated as a single object behave in a similar way to a rigid object that increases its axial ratio progressively while it grows. According to Ghosh & Ramberg (1976), rigid objects with high axial ratios will have decreasing rotation rates once they rotate with their long axis towards parallelism with the flow plane during simple shear deformation. Finite rotation of the studied strain fringes varies from 55° to 110°.

Relative rotation of core-object and fringes

The relative rotation of core-object and fringes can be directly obtained from displacement-controlled fibres and is indicated on the object-centre path (Fig. 4b). Figure 12(c) shows plots of the rotation of core-objects with respect to their fringes versus shear strain. In these plots, the final orientation of the core-object is used as a reference (0° rotation). Relative rotation rates of core-object and fringes show that elongate core-objects with an axial ratio of 2.0 (Fig. 12c, sample IV) tend to rotate at the same rate as their fringes. In contrast, core-objects approaching a circular shape with axial ratios of 1.0–1.4 (Fig. 12c, samples I–III) tend to have faster rotation rates than their fringes with respect to an external reference frame. This is a function of: (1) the shape of core-objects; and (2) the interaction of fringes and core-object. A round core-object will rotate faster than an elongate one if the orientation of its long axis $<45°$ to the flow plane, and core-objects with corners and elongate core-objects cannot rotate easily with respect to their fringes because the corners hinder the rotation. Finite rotation angles of the studied core-objects with axial ratios of 1.0–1.4 are 49° to 75° anticlockwise with respect to their fringes.

DISCUSSION

Strain analysis using single fibres is difficult to apply on fibres in strain fringes from Lourdes because: (1) single fibres do not continue along the whole fringe; (2) not all fibres have displacement-controlled growth; and (3)

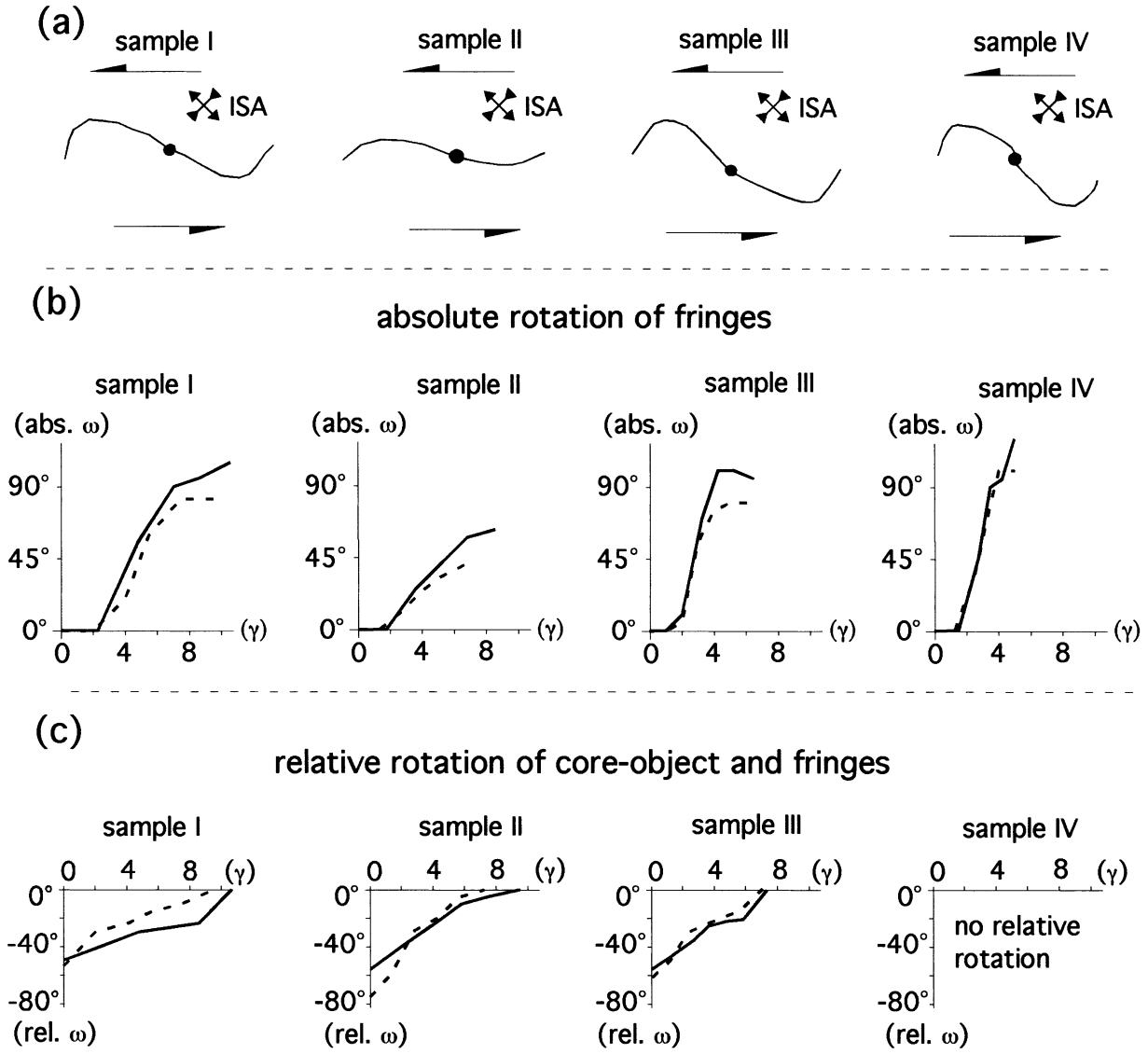

Fig. 12. (a) Orientation of object-centre paths of the four samples studied with respect to ISA. (b) Plots showing estimates of absolute rotation of fringes with respect to ISA versus shear strain obtained from object-centre paths (see Fig. 11). Fringes of samples I to III have first increasing and then decreasing rotation rates. Fringes of samples III and IV rotate faster than fringes of samples I and II. Broken line represents right fringe and solid line left fringe. (c) Plots of core-object rotation relative to their fringes versus shear strain. In these plots, the final orientation of the core-object is used as reference (zero rotation). Sample IV has no core-object rotation relative to its fringes. Samples I to III show finite values of core-object rotation with respect to their fringes of 49° to 75°. Broken line represents right fringe and solid line left fringe.

displacement-controlled fibres of the same age are not parallel if the core-object rotates with respect to its fringes. These problems are probably applicable to most natural strain fringes, especially if progressive deformation is non-coaxial. Therefore, we suggest that object-centre paths should be used for structural analysis of strain fringes instead of single fibres or even instead of sets of fibres.

Object-centre paths can be used to estimate finite bulk strain and rigid body rotation of fringes and core-object. However, care has to be taken because object-centre paths reflect movement of fringes and core-object with respect to each other and not necessarily their movement with respect to ISA or an external reference frame. The opening vector of fringes does not have to be exactly parallel to the extensional ISA during each incremental move (Fig. 12a). Therefore, hook-shaped object-centre paths do not necessarily record a sudden rotation of strain fringes with respect to ISA. They record only a sudden change of the pull apart direction of strain fringes and core-object; these can be just the effect of rotation of the corner of a rectangular core-object in a fringe structure towards the extensional ISA. In this case, fibres will

start to grow at another side of the core-object, and fringes and core-object cannot rotate freely but may rotate at equal rates. Once they rotate at equal rates, object-centre paths will be straight and cannot record rigid body rotation of fringes with respect to ISA. Therefore, one has to keep in mind that the curvature of an object-centre path records the rotation of the oldest segment of a fringe with respect to the orientation of younger segments of the object-centre path. In order to transfer this rotation to the rotation of fringes with respect to an external reference frame (e.g. ISA), the orientation of the incremental opening of the fringes has to be constant with respect to this reference frame over time. If this is not the case, the curvature of an object-centre path will only give estimates on absolute rotation, the reliability of which depends on how much the opening path varies with respect to an external reference frame. It can be assumed that the fringes in our examples opened parallel to the extensional ISA during the early stages of growth. From Fig. 12(a), it can be seen that they did NOT all open parallel to the extensional ISA during the late stages of growth. Therefore, the curvature of the object-centre path can give only *estimates* of fringe rotation with respect to ISA and not absolute values.

It is worth noting that the problems described above might also apply for displacement-controlled (tracking) fibres in extension veins and shear veins, which presumably also record only the relative movement of the walls of veins and not necessarily the orientation of the extensional ISA in all cases.

The two fringes and the core-object of a fringe structure behave like three rigid objects in a weaker matrix. The curvature of the object-centre path does not reflect the rotation of the bulk finite strain ellipsoid, since fringes and core-object can move and rotate relative to each other. A finite strain ellipse cannot rotate more than 45° with respect to ISA during progressive deformation with irrotational ISA and invariable flow parameters. Fibres and object-centre paths *can* curve more than 45° during one non-coaxial deformation event, and a curvature of more than 45° does not necessarily imply polyphase deformation history. The curvature of fibres and object-centre path should not be included in strain analysis since the curvature is a function of a rigid body rotation (Ellis, 1986). Instead, only the length along the object-centre path should be taken since it represents an accumulation of infinitesimally small strain that can be transferred into finite strain. In this paper, it was assumed that the fringe structures developed during a non-coaxial progressive deformation close to simple shear as illustrated earlier in this study. It is worth noting, however, that a polyphase deformation sequence can produce very similar structures and still is a possible alternative explanation for the strain fringes at Lourdes (Aerden, 1996; Mueller *et al*., 2000).

The simulations presented in this paper and in Koehn *et al*. (2000) differ from earlier simulations of fibre patterns in strain fringes of Etchecopar & Malavielle (1987) and Kanagawa (1996). With 'Fringe Growth', progressive fibre growth in fringes can be simulated, whereas Etchecopar & Malavielle (1987) and Kanagawa (1996) simulated the development of fringes using matrix deformation. They assumed that fibres either follow points on the core-object (Etchecopar & Malavielle, 1987) or that they grow parallel to extensional ISA (Kanagawa, 1996). The results presented in Koehn *et al*. (2000) and in this paper have shown that the assumption of Etchecopar & Malavielle (1987) is realistic, whereas the assumption of Kanagawa (1996) leads to errors in the fibre patterns if core-objects rotate relative to their fringes. In contrast to the simulation presented in this paper, where object-centre paths were determined from natural fringe structures and used as input, Etchecopar & Malavielle (1987) and Kanagawa (1996) tried to calculate the progressive development of fringe structures using a 'best fit model' (Etchecopar & Malavielle, 1987) or the laws of Jeffrey (1922) for the rotation of rigid bodies (Kanagawa, 1996). Aerden (1996) tried to reproduce fringe structures from Lourdes with the model of Etchecopar & Malavielle (1987) without success. His major problems were that the program could only produce object-centre paths that did not curve more than 45°, and fibres which were open and did not curve more than 90°, which was inconsistent with observations on natural fringes. Therefore Aerden (1996) concluded that the fringe structures from Lourdes must have developed during a polyphase deformation history. Another possibility is that the inconsistencies between nature and computer model could also lie in the model itself. The following problem arises if the development of a fringe structure is modelled using matrix deformation: a fringe structure consists of three rigid objects, a core-object and its two fringes, where the fringes progressively grow and change their shape. It is not clear how such fringe structures behave during non-coaxial progressive deformation, e.g. can they be treated as one rigid object or as three rigid objects that can rotate relative to each other? Observations presented in this paper and in Koehn *et al*. (2000) have shown that fringes and core-objects do rotate relative to each other which suggests that they behave at least partly like three rigid objects. Therefore, it can be expected that the behaviour of a fringe structure during non-coaxial progressive deformation is more complex than proposed by the models of Etchecopar & Malavielle (1987) and Kanagawa (1996). This could account for the inconsistencies between their computer models and natural examples (Etchecopar & Malavielle, 1987; Aerden, 1996).

The 'Fringe Growth' computer model still has a number of shortcomings. The model is only two-dimensional and it can be expected that there are three-dimensional effects in the fibre patterns, since especially face-controlled and intermediate fibres might grow out of section. However, most of the fibre patterns in the

natural examples are reproduced by the computer growth experiments and, in thin section, most fibres appear to remain in one plane; therefore, we suggest that three-dimensional effects are of minor importance at least in the examples presented in this study.

CONCLUSIONS

The program 'Fringe Growth 2.0' is able to reproduce the complex fibre patterns that are found in natural strain fringes from Lourdes, France. Even though most of the fibres in the fringes show displacement-controlled growth, there are face-controlled and intermediate fibres in the rims of fringes, within displacement-controlled large fibre bands and next to suture lines. Intermediate fibres contain both face-controlled and displacement-controlled fibre boundaries or intermediate fibre boundaries that have face-controlled and displacement-controlled segments along their length. Care has to be taken when interpreting displacement-controlled fibres in strain fringes as fibres that grow parallel to extensional ISA, since the fibres only record relative movement between core-object and fringe.

Object-centre paths should be used for strain analysis instead of single fibres, because these paths separate core-object rotation with respect to its fringes from the translation of fringes away from the core-object and represent all fibres in one fringe. The length along an object-centre path can be interpreted in terms of finite strain. Its curvature gives estimates on rigid body rotation of fringes with respect to an external reference frame. The rotation component cannot be reconstructed with the same reliability as the fringes do not always open parallel to the extensional ISA.

The program 'Fringe Growth 2.0' for the Macintosh is shareware and can be downloaded at: 'http://www.uni-mainz.de/FB/Geo/Geologie/Students/Koehn/FringeGrowthHomep.html'.

ACKNOWLEDGEMENTS

The authors thank H. Fritz and M. Jessell for their careful reviews and their comments that helped to improve the manuscript. This project was made possible by a visit of DK to the Epsilon Earth Processes Simulation Laboratory, Department of Earth Sciences, Monash University, Clayton (Melbourne), Australia and by a visit of DK to the University of Salamanca, Salamanca, Spain. M. Elburg, Beatriz and Tensing are thanked for their hospitality during the visits. The project was funded by the DFG Grant Pa 578/3. We thank M. Jessell, J. Urai and C. Hilgers for their comments and suggestions.

REFERENCES

Aerden, D. G. A. M., 1996. The pyrite-type strain fringes from Lourdes (France): indicators of Alpine thrust kinematics in the Pyrenees. *Journal of Structural Geology*, **18,** 75–91.

Beutner, E. C. & Diegel, F. A., 1985. Determination of fold kinematics from syntectonic fibers in pressure shadows, Martinsburg Slate, New Jersey. *American Journal of Science*, **285,** 16–50.

Beutner, E. C., Fischer, D. M. & Kirkpatrick, J. L., 1988. Kinematics of deformation at a thrust fault ramp (?) from syntectonic fibers in pressure shadows. In: *Geometries and Mechanisms of Thrusting, With Special Reference to the Appalachians* (eds Mitra, G. & Wojtal, S.), pp. 77–88. Special Paper of the Geological Society of America, 222.

Bons, P. D., in press. Development of crystal morphology during unitaxial growth in a progressively widening vein: I. The numerical model. *Journal of Structural Geology*, in press.

Casey, M., Dietrich, D. & Ramsay, J. G., 1983. Methods for determining deformation history for chocolate tablet boudinage with fibrous crystals. *Tectonophysics*, **92,** 211–239.

Clark, M. B., Fisher, D. M. & Chia-Yu, L., 1993. Kinematic analysis of the Hfuehshan Range: a large-scale pop-up structure. *Tectonics*, **12,** 205–217.

Cox, S. F. & Etheridge, M. A., 1983. Crack-seal fibre growth mechanisms and their significance in the development of oriented layer silicate microstructures. *Tectonophysics*, **92,** 147–170.

Durney, D. W. & Ramsay, J. G., 1973. Incremental strains measured by syntectonic crystal growths. In: *Gravity and Tectonics* (eds DeJong, K. A. & Scholten, R.), pp. 67–95. Wiley, New York.

Elliot, D., 1972. Deformation paths in structural geology. *Bulletin of the Geological Society of America*, **83,** 2621–2638.

Ellis, M. A., 1986. The determination of progressive deformation histories from antitaxial syntectonic crystal fibres. *Journal of Structural Geology*, **8,** 701–709.

Etchecopar, A. & Malavielle, J., 1987. Computer models of pressure shadows: a method for strain measurement and shear sense determination. *Journal of Structural Geology*, **9,** 667–677.

Fisher, D. M., 1990. Orientation history and rheology in slates, Kodiak and Afognak Islands, Alaska. *Journal of Structural Geology*, **12,** 483–498.

Fisher, D. & Anastasio, D. J., 1994. Kinematic analysis of a large-scale leading edge fold, Lost River Range, Idaho. *Journal of Structural Geology*, **16,** 337–354.

Ghosh, S. K. & Ramberg, H., 1976. Reorientation of inclusions by combination of pure shear and simple shear. *Tectonophysics*, **34,** 1–70.

Hedlund, C. A., Anastasio, D. J. & Fisher, D. M., 1994. Kinematics of fault-related folding in a duplex, Lost River Range, Idaho, U.S.A. *Journal of Structural Geology*, **16,** 571–584.

Hilgers, C., Koehn, D., Bons, P. D. & Urai, J. L., in press. Development of crystal morphology during unitaxial growth in a progressively widening vein: II. Numerical simulations of the evolution of antitaxial fibrous veins. *Journal of Structural Geology*, in press.

Hilgers, C., Urai, J. L., Post, A. D. & Bons, P. D., 1997. Fibrous vein microstructure: experimental and numerical simulation. *Aardkundige Mededelingen*, **8,** 107–109.

Jeffrey, G. B., 1922. The motion of ellipsoidal particles immersed in a viscous fluid. *Proceedings of the Royal Society of London.*, **A102,** 161–179.

Kanagawa, K., 1996. Simulated pressure fringes, vorticity, and progressive deformation. In: *Structural Geology and Personal Computers. Computer Methods in the Geosciences, 15* (ed. De Paor, D. G.), pp. 259–283. Pergamon, Elsevier, Oxford.

Koehn, D., Hilgers, C., Bons, P. D. & Passchier, C. W., 2000. Numerical simulation of fibre growth in antitaxial strain fringes. *Journal of Structural Geology*, **22,** 1311–1324.

Koehn, D., Passchier, C. W. & Bons, P. D., 1999. Kinematic analysis of strain fringes. *Journal of Conference Abstracts*, **4 (EUG 10),** 830.

Means, W. D., 1976. *Stress and Strain*. Springer, Heidelberg.

Muegge, O., 1928. Ueber die Entstehung faseriger Minerale und ihrer Aggregationsformen. *Neues Jahrbuch für Mineralogie, Geologie und Paläontologie*, **58A,** 303–438.

Mueller, W., Aerden, D. & Halliday, A. N., 2000. Isotopic dating of strain fringe increments: duration and rates of deformation in shear zones. *Science*, **288,** 2195–2198.
Pabst, A., 1931. 'Pressure shadows' and the measurement of the orientation in rocks. *Journal of the Mineralogical Society of America*, **16,** 55–70.
Passchier, C. W. & Trouw, R. A. J., 1996. *Microtectonics*. Springer, Heidelberg.
Ramsay, J. G. & Huber, M. I., 1983. *The Techniques of Modern Structural Geology, 1: Strain Analysis*. Academic Press, London.
Sample, J. C. & Fisher, D. M., 1986. Duplex accretion and underplating in an ancient accretionary complex, Kodiak Islands, Alaska. *Geology*, **14,** 160–163.
Selkman, S. O., 1983. Stress and displacement distributions around pyrite grains. *Journal of Structural Geology*, **5,** 47–52.
Spencer, S., 1991. The use of syntectonic fibres to determine strain estimates and deformation paths: an appraisal. *Tectonophysics*, **194,** 13–34.
Urai, J. L., Williams, P. F. & Van Roermund, H. L. M., 1991. Kinematics of crystal growth in syntectonic fibrous veins. *Journal of Structural Geology*, **13,** 823–836.
Wickham, J. S., 1973. An estimate of strain increments in a naturally deformed carbonate rock. *American Journal of Science*, **237,** 23–47.
Wickham, J. S. & Anthony, M., 1977. Strain paths and folding of carbonate rocks near Blue Ridge, central Appalachians. *Bulletin of the Geological Society of America*, **88,** 920–924.
Zwart, H. J. & Oele, J. A., 1966. Rotated magnetite crystals from the Rocroi Massif (Ardennes). *Geologie en Mijnbouw*, **45,** 70–74.

Received 13 April 2000; revision accepted 9 October 2000